Supporting Information

Two Robust Polyoxovanadate Clusters Having a Square-Prism $V_{10}O_x$ Core for Efficient Catalysis of Benzene Hydroxylation to Phenol

Ji-Lei Wang, Ling-Xi Xu, Qin Wang, Pin-Fang Yan, Xin-Lian Chen, Ting Jin, Hua Mei,* and Yan Xu*

State Key Laboratory of Materials-Oriented Chemical Engineering, College of Chemical Engineering, Nanjing Tech University, Nanjing 211816, P.R. China.

Corresponding Author* yanxu@njtech.edu.cn

Table of contents

1. Experimental Section

1.1 Procedure for benzene hydroxylation to phenol
1.2 X-ray crystallography
Table S1. Crystal data and structure refinements for **V_{10}-BTA** and **V_{10}-CBTA**.
Table S2. Selected bond lengths (Å) and bond angles (deg) for **V_{10}-BTA**.
Table S3. Selected bond lengths (Å) and bond angles (deg) for **V_{10}-CBTA**.
Table S4. The BVS calculation results of V atoms in **V_{10}-BTA** and **V_{10}-CBTA**.
Figure S1. The pictures of crystal morphology for (a) **V_{10}-BTA**, and (b) **V_{10}-CBTA**.

2. Crystal Structure

Figure S2. The ball and stick model for (a) **V_{10}-BTA**, and (b) **V_{10}-CBTA**.
Figure S3. (a) Polyhedral structural mode for **V_{10}-BTA** without H atoms. (b) Polyhedral structural mode for main structure in **V_{10}-BTA**.
Figure S4. The front (a), top (b), and side (c) of polyhedral structural mode for main structure in **V_{10}-BTA**.
Figure S5. (a) Structure of $\{V^{III}V^{IV}_4\}$ unit; (b) the coordination environment of O9 (OH) in **V_{10}-BTA**.
Figure S6. The coordination model of V1, V2, V3, V4, V5 in **V_{10}-BTA**.
Figure S7. (a) Ball-and-stick and (b) polyhedral structural modes for V_{10} core in **V_{10}-CBTA**; Ball-and-stick structural mode for (c) **V_{10}-CBTA**.
Figure S8. Representation of the coordination environment for V atoms in **V_{10}-CBTA**.
Figure S9. The stacking model of **V_{10}-BTA**.
Figure S10. The stacking model of **V_{10}-CBTA**.
Figure S11. (a) Asymmetric unit of **V_{10}-en**; (b) ball-and-stick and (c) polyhedral structural modes of V_{10} unit in **V_{10}-en**.

3. Characterization

Figure S12. The powder XRD patterns of **V_{10}-BTA**.
Figure S13. The Powder XRD pattern of **V_{10}-CBTA**.
Figure S14. The IR spectrum of **V_{10}-BTA**.
Figure S15. The IR spectrum of **V_{10}-CBTA**.
Figure S16. The TGA thermogram of as-synthesized **V_{10}-CBTA**.

4. Oxidation of Sulfides

Scheme S1. Reaction Scheme for MPS Oxidation.
Figure S17. The relationships between the conversion/selectivity of oxidative products (RR'SO: methyl phenyl sulfoxide; RR'SO_2: methyl phenyl sulfone) and (a) the solvent, (b) the dosage of H_2O_2 (oxidant agent), (c) the dosage of catalyst **V_{10}-BTA**, and (d) the reaction time.

5. Benzene Hydroxylation to Phenol

Figure S18. Catalytic oxidative reaction of benzene using **V_{10}-BTA** and **V_{10}-CBTA** as catalysts with respect to a catalyst-free (blank) and a H_2O_2-free trial. Reaction conditions: benzene (1 mL), 30% H_2O_2 (3 mL), catalyst (25 mg), CH_3CN (5.0 mL), 60 °C, 6 hours.
Figure S19. Catalytic dynamic of the hydroxylation of benzene by **V_{10}-BTA** (blue), and filter out the catalyst during the reaction (red).
Figure S20. XRD pattern of **V_{10}-BTA** after several cycles in the hydroxylation of benzene.
Figure S21. Infrared spectra of **V_{10}-BTA** after several cycles in the hydroxylation of benzene.
Table S5. The comparison of benzene hydroxylation of some reported POM-based catalysts.

6. References

1. Experimental Section

1.1 Procedure for benzene hydroxylation to phenol

In a typical run of H_2O_2-mediated benzene hydroxylation, the reaction tube with a volume of 25 mL (2 × 20 cm) was subsequently charged with the catalyst (0.1 g), CH_3CN (5 mL), acetic acid (1 mL), and benzene and then heated at 60 °C. H_2O_2 was introduced smoothly into the reaction tube using a syringe pump. The qualitative product identification was performed by using a Triple-Axis detector on an Agilent 7920A/5975 Bruker Scion 436 gas chromatography-mass spectrometry (GC-MS). The quantitative product analysis was carried out by using the liquid chromatography Thermo U-3000. The internal standard employed in the experiment was biphenyl (0.05 g). After the reaction, the catalyst was retrieved and directly introduced into the subsequent experiment to examine its recyclability. Various other arenes were used as the substrates to study the scope. Possible by-products such as hydroquinone and benzoquinone were also analyzed using the same method. The calculation formula for phenol selectivity was as follows:

Conversion of benzene (%) = (moles of benzene initially used - moles of benzene present in the final mixture)/(moles of benzene initially used) × 100

The yield of phenol (%) = (mmol phenol)/(initial mmol benzene) × 100

The selectivity of phenol (%) = (mmol phenol)/(mmol phenol + mmol by products)

Kinetic isotope effect experiments were conducted to study the effect of C–H activation by replacing the benzene with deuterated benzene to calculate K_H/K_D values (K_H and K_D represent the reaction rates by using benzene and deuterated benzene respectively).

Reusability was evaluated in a five-run recycling test. After each run, the catalyst was isolated, washed with deionized water and anhydrous ethanol respectively three times, dried at 70 °C overnight, and then charged into the next run.

1.2 X-ray crystallography

The crystal XRD data of three as-synthesized clusters was collected at 296(3) K on Bruker Apex II CCD with Mo-Kα radiation (λ = 0.71073 Å). The SHELX software package was utilized to resolve and refine the structures of $\mathbf{V_{10}}$ clusters through the direct methods and full-matrix least-squares methods on F^2 in the SHELX-2018/3 program package. In addition, all the non-H atoms were refined by anisotropic thermal parameters. The detailed crystallographic data for two $\mathbf{V_{10}}$ clusters are summarized in Table S1. Selected bond distance (Å), angles (°) and hydrogen bonds were provided in Tables S2-S3. Crystallographic data have been deposited with the Cambridge Crystallographic Data Centre (CCDC) as 2376599 (**$\mathbf{V_{10}}$-BTA**), and 2376600 (**$\mathbf{V_{10}}$-CBTA**).

Table S1. Crystal data and structure refinements for **$\mathbf{V_{10}}$-BTA** and **$\mathbf{V_{10}}$-CBTA**.

Compound	**V_{10}-BTA**	**V_{10}-CBTA**
Formula	$C_{62}H_{82}N_{24}O_{26}V_{10}$	$C_{58}H_{60}Cl_8N_{24}O_{24}V_{10}$
Formula weight	2088.91	2270.30
T (K)	193(2)	296(2)
Crystal system	Triclinic	Triclinic
Space group	P-1	P-1
a (Å)	13.1203(16)	13.0918(17)
b (Å)	13.1204(16)	14.0964(18)
c (Å)	14.600(3)	14.1870(18)
α (°)	110.362(2)	68.963(2)
β (°)	110.362(2)	76.955(2)
γ (°)	97.15	62.586(2)
V (Å^3)	2121.0(5)	2163.5(5)
Z	1	1
D_c (mg/m^3)	1.635	1.743
μ (mm^{-1})	1.135	1.358
F (000)	1060	1134
θ range (°)	1.724-25.499	1.703-25.025
	$-15\leq h\leq 15$	$-15\leq h\leq 15$
Limiting indices	$-15\leq k\leq 15$	$-16\leq k\leq 16$
	$-17\leq l\leq 17$	$-15\leq l\leq 16$
Reflections collected / unique	22023 / 7734	15664 / 7574
R (int)	0.0549	0.0354
Data / restraints / parameters	7734 / 83 / 596	7574 / 30 / 602
GOF	1.103	1.045
R_1[a], wR_2[b] [$I>2\sigma(I)$]	0.0718, 0.2037	0.0709, 0.2244
R_1, wR_2 (all data)	0.1023, 0.2245	0.0953, 0.2427

Table S2. Selected bond lengths (Å) and bond angles (deg) for **V_{10}-BTA**.

V(1)-O(5)	1.594(4)	V(3)-N(3)	2.094(5)
V(1)-O(4)	1.967(5)	V(3)-N(12)	2.121(5)
V(1)-O(7)	2.000(4)	V(3)-O(9)	2.292(4)
V(1)-N(4)	2.101(4)	V(4)-O(6)	1.597(4)
V(1)-N(9)#1	2.113(5)	V(4)-O(1)	1.986(5)
V(1)-O(9)	2.285(4)	V(4)-O(3)	1.988(4)
V(2)-O(9)	1.765(4)	V(4)-N(6)	2.104(5)
V(2)-O(10)	1.903(4)	V(4)-N(10)#1	2.134(5)
V(2)-O(11)	1.952(3)	V(4)-O(10)#1	2.243(4)
V(2)-O(11)#1	1.958(3)	V(5)-O(2)	1.585(4)
V(2)-N(8)#1	2.143(4)	V(5)-O(3)	2.002(4)
V(2)-N(11)	2.147(4)	V(5)-O(1)	2.017(5)
V(3)-O(8)	1.597(4)	V(5)-N(1)	2.122(5)
V(3)-O(4)	1.982(4)	V(5)-N(7)	2.129(5)
V(3)-O(7)	1.984(4)	V(5)-O(10)#1	2.229(4)
O(5)-V(1)-O(4)	108.6(2)	O(7)-V(3)-N(12)	91.15(17)
O(5)-V(1)-O(7)	106.82(19)	N(3)-V(3)-N(12)	93.08(18)
O(4)-V(1)-O(7)	72.96(17)	O(8)-V(3)-O(9)	175.20(19)
O(5)-V(1)-N(4)	97.2(2)	O(4)-V(3)-O(9)	74.96(16)
O(4)-V(1)-N(4)	94.80(18)	O(7)-V(3)-O(9)	74.23(14)
O(7)-V(1)-N(4)	155.47(18)	N(3)-V(3)-O(9)	83.76(16)
O(5)-V(1)-N(9)#1	97.5(2)	N(12)-V(3)-O(9)	78.57(15)
O(4)-V(1)-N(9)#1	152.06(18)	O(6)-V(4)-O(1)	108.6(2)
O(7)-V(1)-N(9)#1	90.36(18)	O(6)-V(4)-O(3)	107.3(2)
N(4)-V(1)-N(9)#1	91.62(19)	O(1)-V(4)-O(3)	74.8(2)
O(5)-V(1)-O(9)	176.0(2)	O(6)-V(4)-N(6)	97.0(2)
O(4)-V(1)-O(9)	75.41(16)	O(1)-V(4)-N(6)	94.14(19)
O(7)-V(1)-O(9)	74.12(14)	O(3)-V(4)-N(6)	155.40(18)
N(4)-V(1)-O(9)	82.32(16)	O(6)-V(4)-N(10)#1	95.8(2)
N(9)#1-V(1)-O(9)	78.56(16)	O(1)-V(4)-N(10)#1	153.79(19)
O(9)-V(2)-O(10)	161.65(17)	O(3)-V(4)-N(10)#1	89.23(19)
O(9)-V(2)-O(11)	99.38(16)	N(6)-V(4)-N(10)#1	92.10(18)
O(10)-V(2)-O(11)	95.19(16)	O(6)-V(4)-O(10)#1	176.97(19)
O(9)-V(2)-O(11)#1	98.68(16)	O(1)-V(4)-O(10)#1	74.40(16)
O(10)-V(2)-O(11)#1	94.85(15)	O(3)-V(4)-O(10)#1	72.78(16)
O(11)-V(2)-O(11)#1	79.67(15)	N(6)-V(4)-O(10)#1	83.16(15)
O(9)-V(2)-N(8)#1	84.70(18)	N(10)#1-V(4)-O(10)#1	81.12(15)
O(10)-V(2)-N(8)#1	82.94(17)	O(2)-V(5)-O(3)	106.5(2)
O(11)-V(2)-N(8)#1	169.40(15)	O(2)-V(5)-O(1)	109.8(2)
O(11)#1-V(2)-N(8)#1	90.07(15)	O(3)-V(5)-O(1)	73.9(2)
O(9)-V(2)-N(11)	84.83(17)	O(2)-V(5)-N(1)	97.2(2)
O(10)-V(2)-N(11)	84.02(16)	O(3)-V(5)-N(1)	155.55(18)
O(11)-V(2)-N(11)	90.14(15)	O(1)-V(5)-N(1)	92.8(2)

O(11)#1-V(2)-N(11)	169.62(16)	O(2)-V(5)-N(7)	95.9(2)
N(8)#1-V(2)-N(11)	100.01(16)	O(3)-V(5)-N(7)	90.0(2)
O(8)-V(3)-O(4)	109.6(2)	O(1)-V(5)-N(7)	152.58(19)
O(8)-V(3)-O(7)	105.52(19)	N(1)-V(5)-N(7)	93.53(19)
O(4)-V(3)-O(7)	72.97(18)	O(2)-V(5)-O(10)#1	175.8(2)
O(8)-V(3)-N(3)	97.1(2)	O(3)-V(5)-O(10)#1	72.84(15)
O(4)-V(3)-N(3)	93.10(18)	O(1)-V(5)-O(10)#1	74.15(17)
O(7)-V(3)-N(3)	156.29(17)	N(1)-V(5)-O(10)#1	83.95(16)
O(8)-V(3)-N(12)	96.7(2)	N(7)-V(5)-O(10)#1	80.01(16)
O(4)-V(3)-N(12)	151.96(18)		

Symmetry transformations used to generate equivalent atoms:

#1 -x+1, -y, -z+1

Table S3. Selected bond lengths (Å) and bond angles (deg) for **V_{10}-CBTA**.

V(1)-O(1)	1.581(4)	V(3)-N(10)	2.140(5)
V(1)-O(8)	1.977(4)	V(3)-O(10)	2.252(4)
V(1)-O(5)	1.994(4)	V(4)-O(4)	1.582(4)
V(1)-N(4)#1	2.127(5)	V(4)-O(7)	1.989(4)
V(1)-N(1)	2.129(5)	V(4)-O(6)	1.990(4)
V(1)-O(10)	2.258(4)	V(4)-N(6)	2.125(5)
V(2)-O(2)	1.584(4)	V(4)-N(12)	2.138(5)
V(2)-O(7)	1.975(4)	V(4)-O(12)	2.253(4)
V(2)-O(6)	1.986(4)	V(5)-O(10)	1.830(4)
V(2)-N(3)	2.132(5)	V(5)-O(12)	1.866(4)
V(2)-N(7)#1	2.135(5)	V(5)-O(11)#1	1.957(3)
V(2)-O(12)	2.245(4)	V(5)-O(11)	1.960(4)
V(3)-O(3)	1.585(4)	V(5)-O(9)	2.121(4)
V(3)-O(8)	1.967(4)	V(5)-O(9)#1	2.157(4)
V(3)-O(5)	2.001(4)	V(5)-N(11)	2.166(4)
V(3)-N(8)	2.131(5)	V(5)-N(2)	2.174(5)
O(1)-V(1)-O(8)	107.3(2)	N(10)-V(3)-O(10)	79.79(16)
O(1)-V(1)-O(5)	107.8(2)	O(4)-V(4)-O(7)	108.4(2)
O(8)-V(1)-O(5)	74.86(18)	O(4)-V(4)-O(6)	107.0(2)
O(1)-V(1)-N(4)#1	96.3(2)	O(7)-V(4)-O(6)	75.74(17)
O(8)-V(1)-N(4)#1	92.54(19)	O(4)-V(4)-N(6)	97.0(2)
O(5)-V(1)-N(4)#1	155.20(18)	O(7)-V(4)-N(6)	92.13(19)
O(1)-V(1)-N(1)	97.6(2)	O(6)-V(4)-N(6)	155.44(17)
O(8)-V(1)-N(1)	153.76(18)	O(4)-V(4)-N(12)	96.4(2)
O(5)-V(1)-N(1)	90.00(19)	O(7)-V(4)-N(12)	154.03(18)
N(4)#1-V(1)-N(1)	92.8(2)	O(6)-V(4)-N(12)	89.99(18)
O(1)-V(1)-O(10)	176.6(2)	N(6)-V(4)-N(12)	92.37(19)
O(8)-V(1)-O(10)	74.88(16)	O(4)-V(4)-O(12)	176.9(2)
O(5)-V(1)-O(10)	75.26(15)	O(7)-V(4)-O(12)	74.63(16)
N(4)#1-V(1)-O(10)	80.89(16)	O(6)-V(4)-O(12)	74.43(15)
N(1)-V(1)-O(10)	80.65(17)	N(6)-V(4)-O(12)	81.84(16)
O(2)-V(2)-O(7)	106.8(2)	N(12)-V(4)-O(12)	80.73(16)
O(2)-V(2)-O(6)	107.2(2)	O(10)-V(5)-O(12)	161.69(18)
O(7)-V(2)-O(6)	76.12(18)	O(10)-V(5)-O(11)#1	97.70(16)
O(2)-V(2)-N(3)	97.7(2)	O(12)-V(5)-O(11)#1	96.42(16)
O(7)-V(2)-N(3)	154.62(18)	O(10)-V(5)-O(11)	98.33(16)
O(6)-V(2)-N(3)	90.42(18)	O(12)-V(5)-O(11)	95.81(16)
O(2)-V(2)-N(7)#1	96.4(2)	O(11)#1-V(5)-O(11)	78.69(15)
O(7)-V(2)-N(7)#1	89.60(18)	O(10)-V(5)-O(9)	54.98(15)
O(6)-V(2)-N(7)#1	155.03(18)	O(12)-V(5)-O(9)	143.33(16)
N(3)-V(2)-N(7)#1	94.42(19)	O(11)#1-V(5)-O(9)	57.02(14)
O(2)-V(2)-O(12)	177.6(2)	O(11)-V(5)-O(9)	57.22(14)
O(7)-V(2)-O(12)	75.06(16)	O(10)-V(5)-O(9)#1	144.83(17)

O(6)-V(2)-O(12)	74.68(16)	O(12)-V(5)-O(9)#1	53.48(16)
N(3)-V(2)-O(12)	80.70(17)	O(11)#1-V(5)-O(9)#1	56.63(14)
N(7)#1-V(2)-O(12)	81.95(16)	O(11)-V(5)-O(9)#1	56.34(14)
O(3)-V(3)-O(8)	108.7(2)	O(9)-V(5)-O(9)#1	89.86(14)
O(3)-V(3)-O(5)	106.1(2)	O(10)-V(5)-N(11)	84.02(17)
O(8)-V(3)-O(5)	74.93(19)	O(12)-V(5)-N(11)	84.10(17)
O(3)-V(3)-N(8)	96.7(2)	O(11)#1-V(5)-N(11)	169.94(18)
O(8)-V(3)-N(8)	90.57(19)	O(11)-V(5)-N(11)	91.26(16)
O(5)-V(3)-N(8)	155.91(18)	O(9)-V(5)-N(11)	117.61(16)
O(3)-V(3)-N(10)	96.5(2)	O(9)#1-V(5)-N(11)	117.22(16)
O(8)-V(3)-N(10)	153.97(18)	O(10)-V(5)-N(2)	84.20(18)
O(5)-V(3)-N(10)	91.92(19)	O(12)-V(5)-N(2)	83.73(17)
N(8)-V(3)-N(10)	93.29(19)	O(11)#1-V(5)-N(2)	92.00(17)
O(3)-V(3)-O(10)	176.1(2)	O(11)-V(5)-N(2)	170.59(17)
O(8)-V(3)-O(10)	75.21(16)	O(9)-V(5)-N(2)	118.66(17)
O(5)-V(3)-O(10)	75.27(15)	O(9)#1-V(5)-N(2)	117.17(16)
N(8)-V(3)-O(10)	82.54(16)	N(11)-V(5)-N(2)	98.03(19)

Symmetry transformations used to generate equivalent atoms:
#1 -x+1, -y+1, -z+1

Table S4. The BVS calculation [1] results of V atoms in **V_{10}-BTA** and **V_{10}-CBTA**.

Compound	Code	Bond Valence
V_{10}-BTA	V1	3.90
	V2	3.32
	V3	3.89
	V4	3.86
	V5	3.83
V_{10}-CBTA	V1	3.91
	V2	3.93
	V3	3.89
	V4	3.90
	V5	4.36

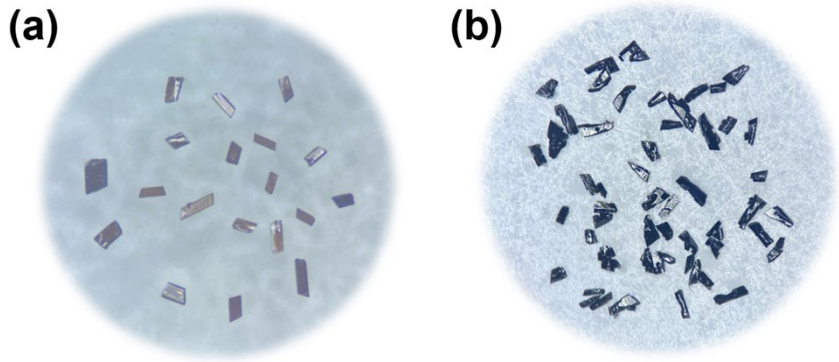

Figure S1. The pictures of crystal morphology for (a) **V_{10}-BTA**, and (b) **V_{10}-CBTA**.

2. Crystal Structure

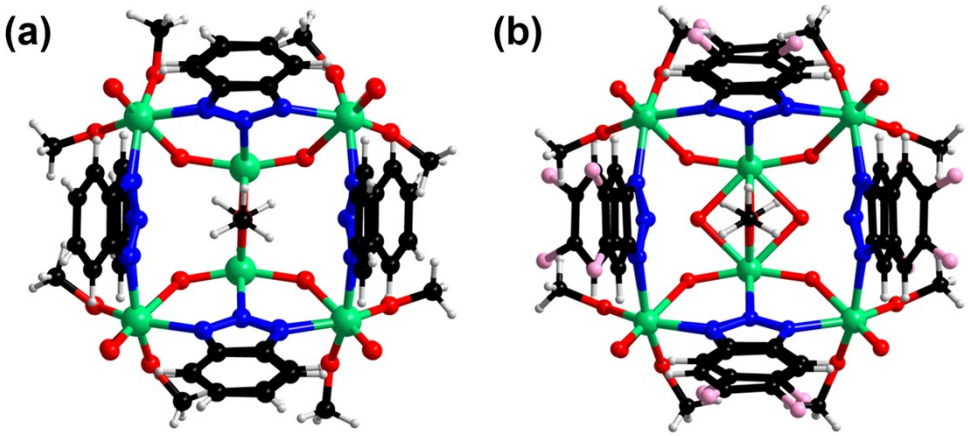

Figure S2. The ball and stick model for (a) **V_{10}-BTA**, and (b) **V_{10}-CBTA**.

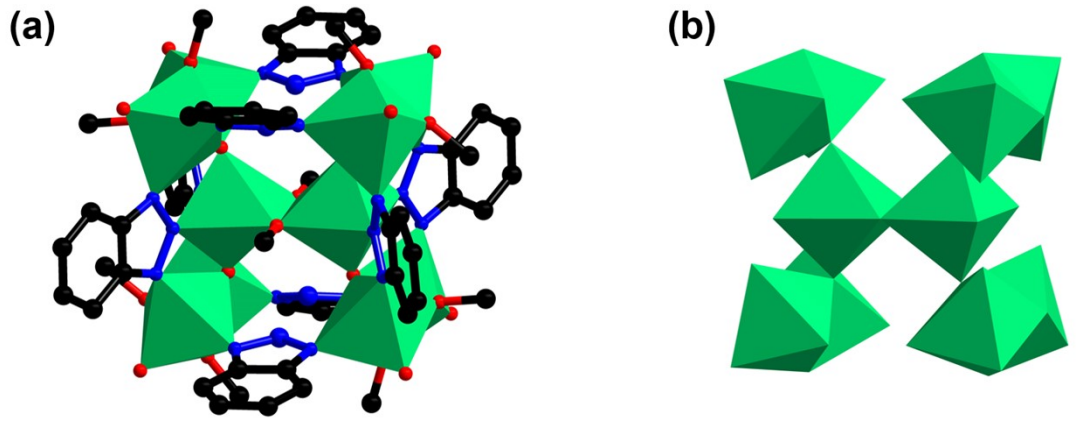

Figure S3. (a) Polyhedral structural mode for **V_{10}-BTA** without H atoms. (b) Polyhedral structural mode for main structure in **V_{10}-BTA**.

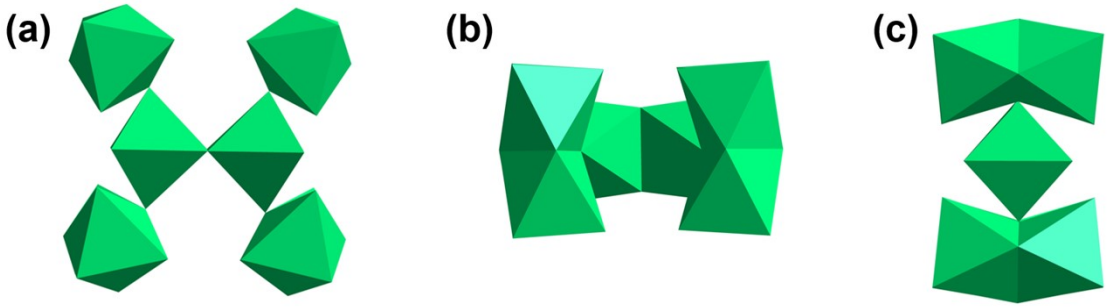

Figure S4. The front (a), top (b), and side (c) of polyhedral structural mode for main structure in **V_{10}-BTA**.

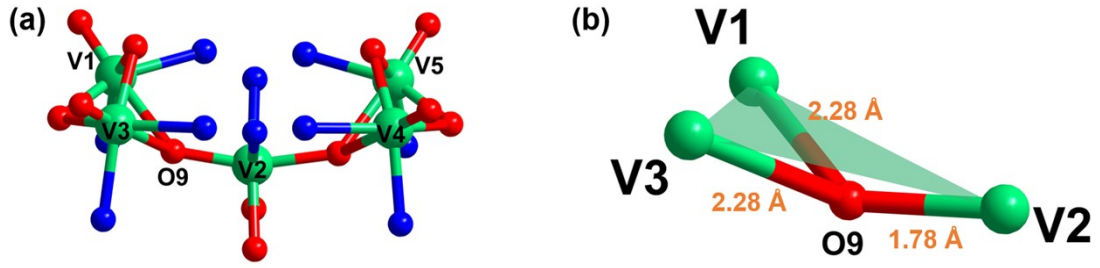

Figure S5. (a) Structure of $\{V^{III}V^{IV}_4\}$ unit; (b) the coordination environment of O9 (OH) in **V_{10}-BTA**.

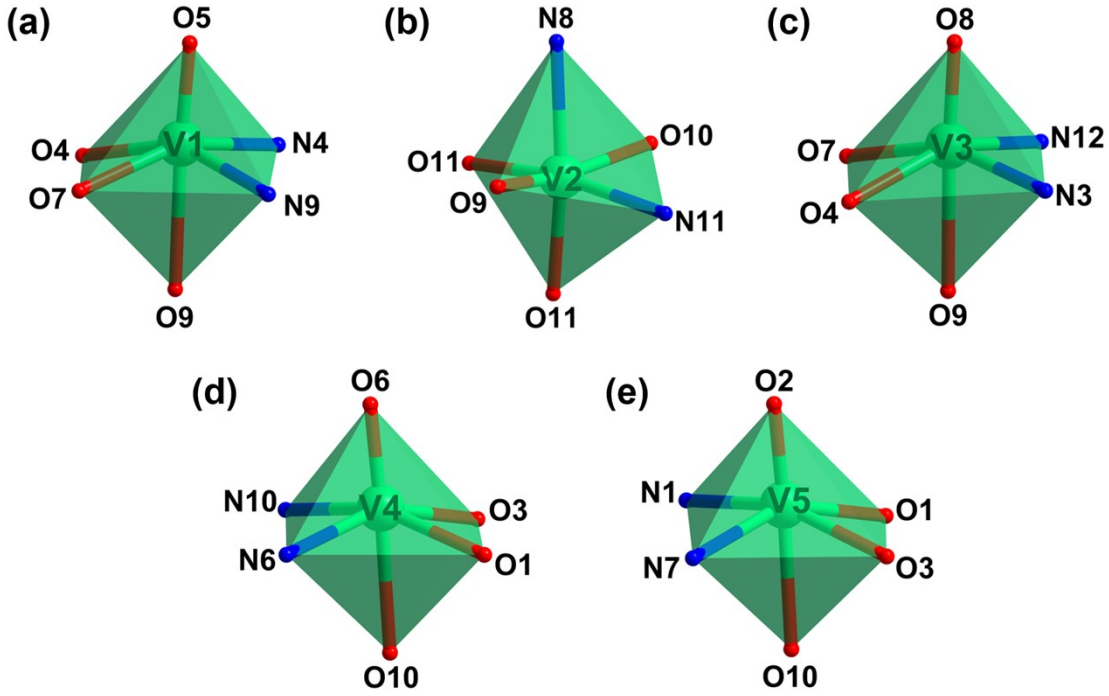

Figure S6. The coordination model of V1, V2, V3, V4, V5 in **V_{10}-BTA**.

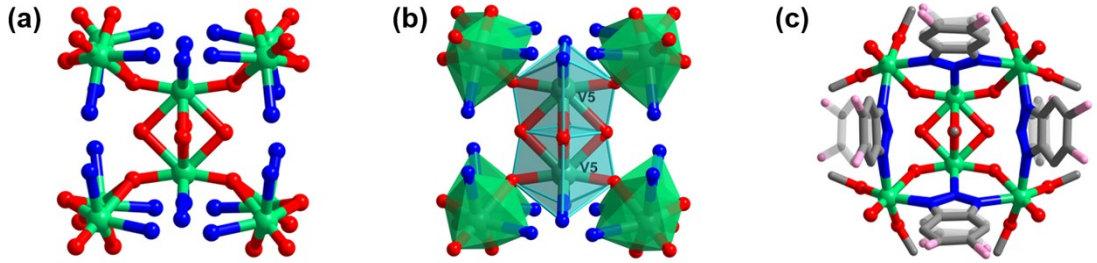

Figure S7. (a) Ball-and-stick and (b) polyhedral structural modes for V_{10} core in **V_{10}-CBTA**; Ball-and-stick structural mode for (c) **V_{10}-CBTA**.

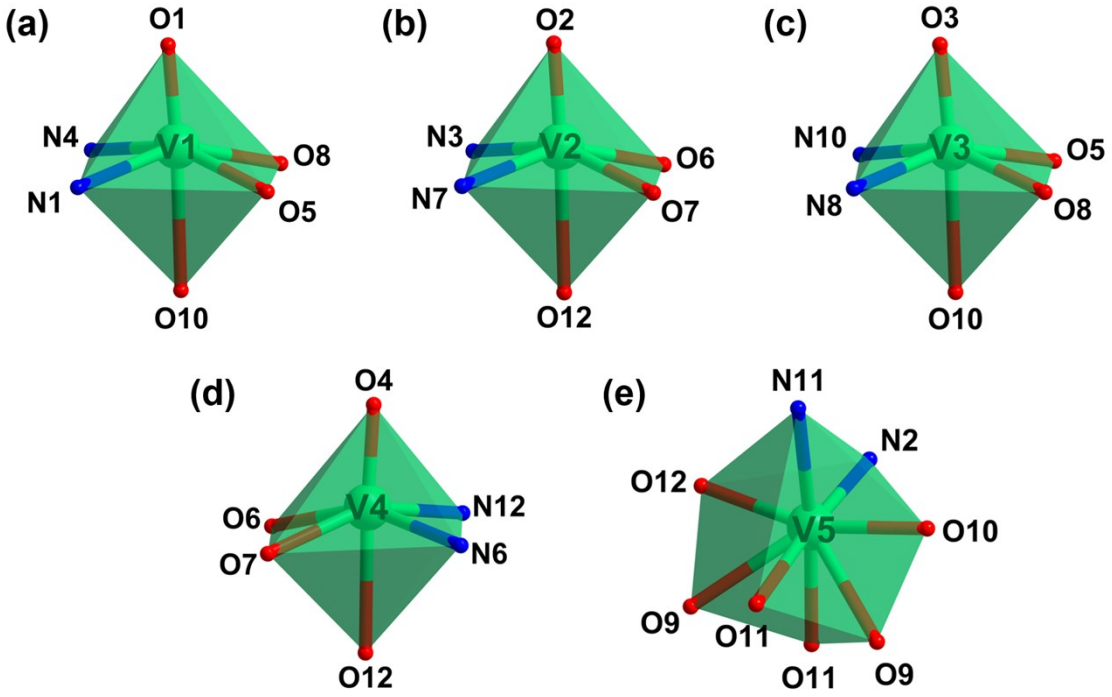

Figure S8. Representation of the coordination environment for V atoms in **V_{10}-CBTA**.

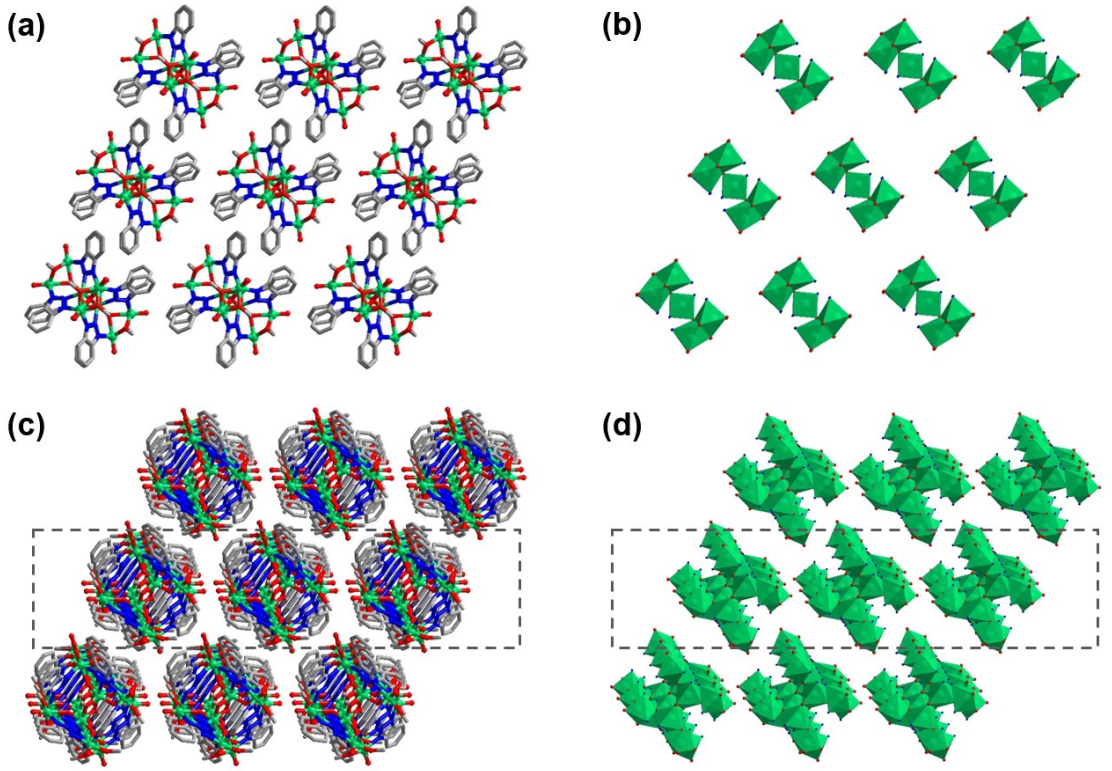

Figure S9. The stacking model of **V_{10}-BTA**.

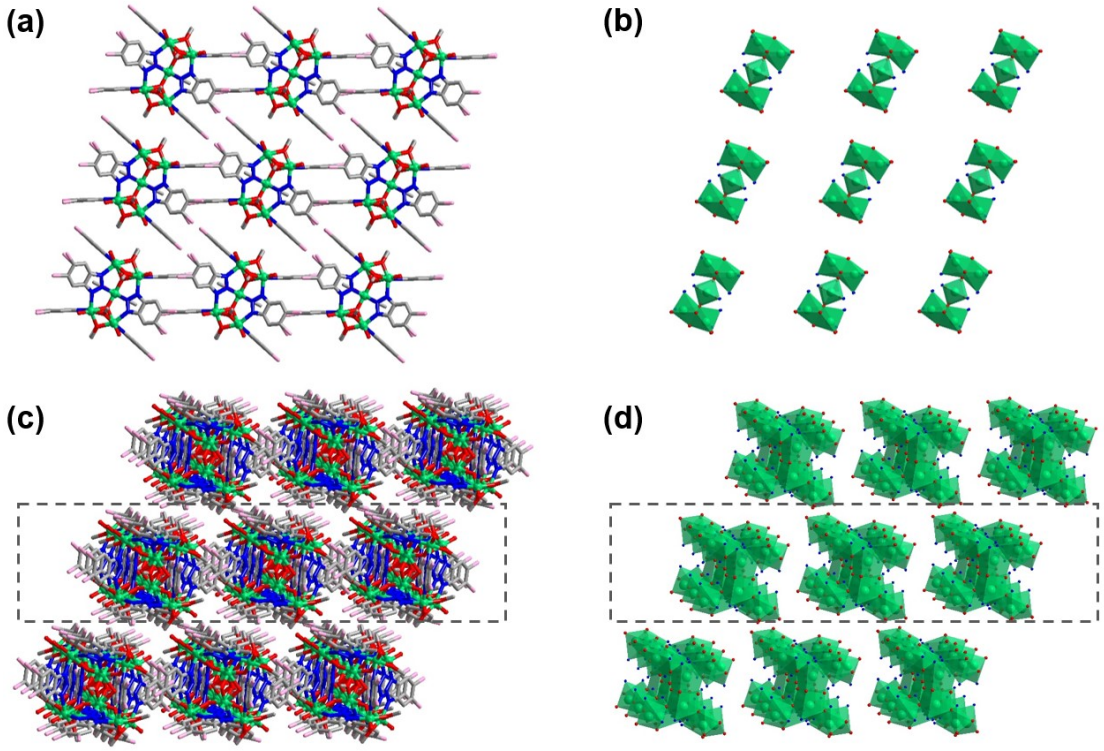

Figure S10. The stacking model of **V_{10}-CBTA**.

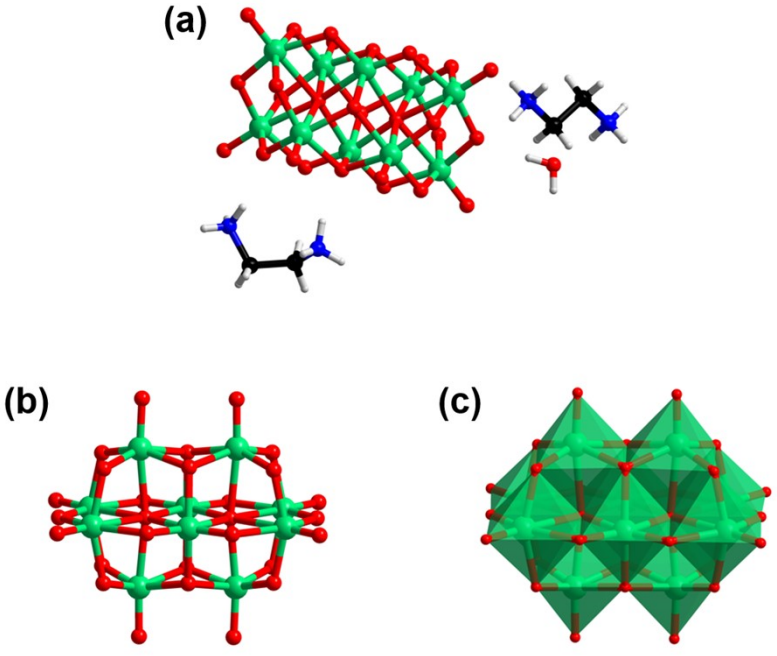

Figure S11. (a) Asymmetric unit of **V_{10}-en**; (b) ball-and-stick and (c) polyhedral structural modes of V_{10} unit in **V_{10}-en**.

3. Characterization

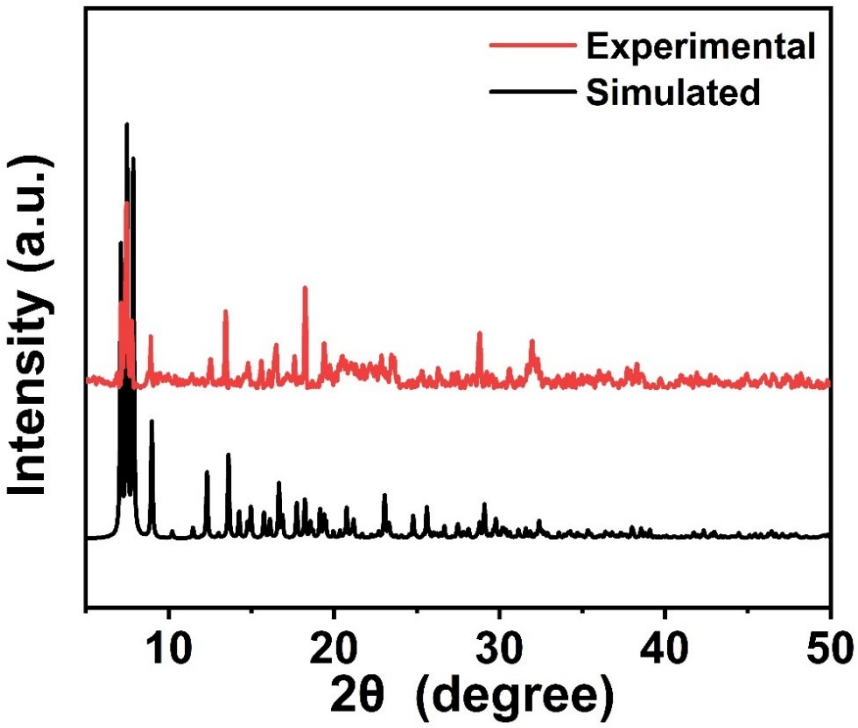

Figure S12. The powder XRD patterns of **V_{10}-BTA**.

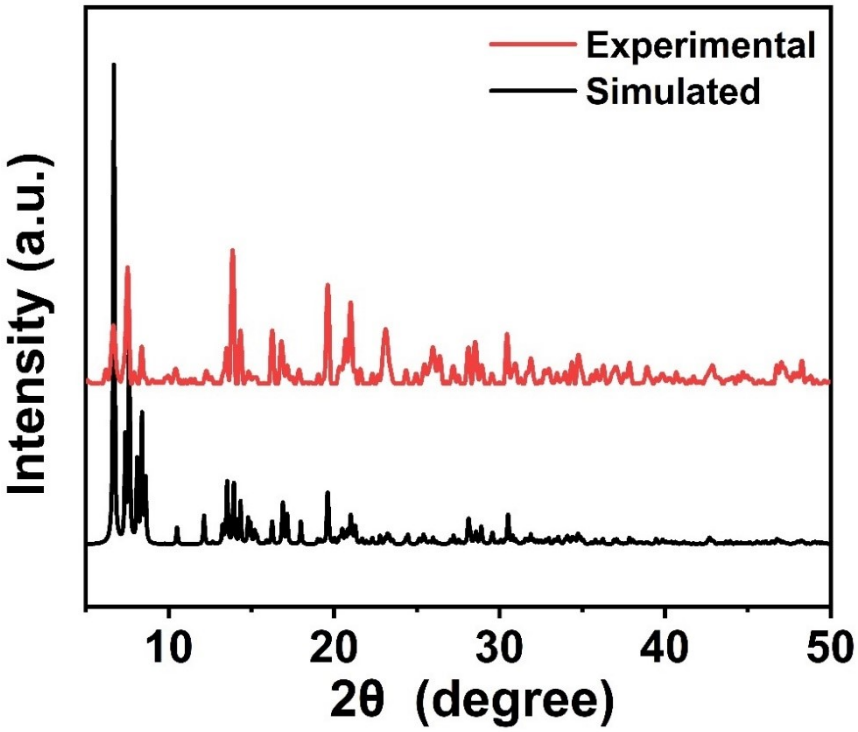

Figure S13. The powder XRD patterns of **V_{10}-CBTA**.

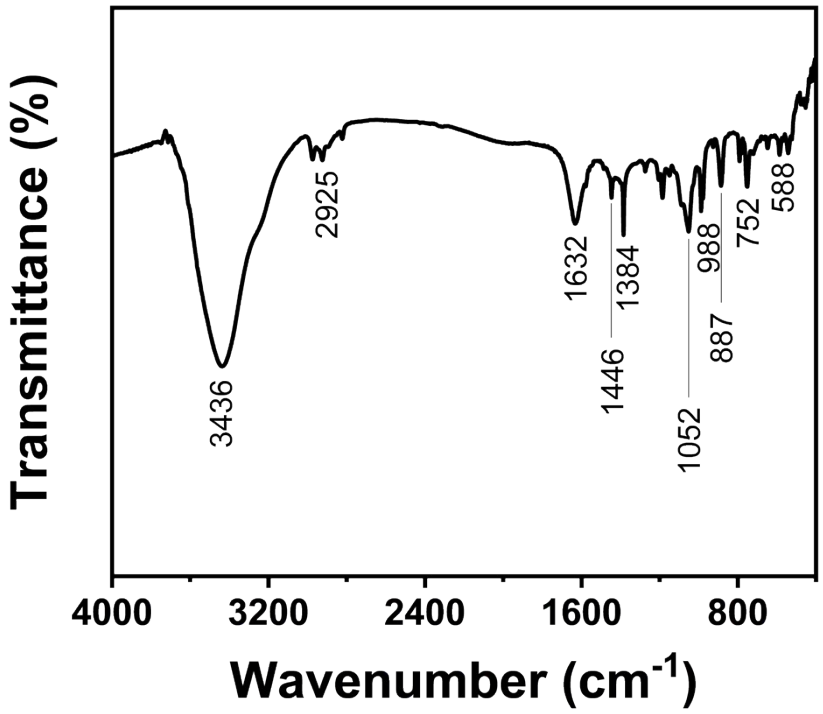

Figure S14. The IR spectrum of **V_{10}-BTA**.

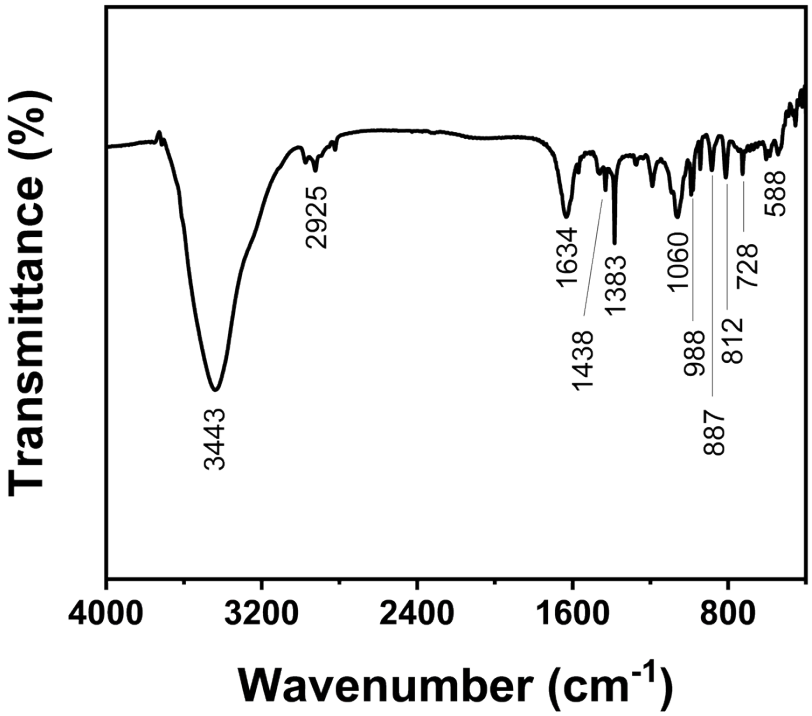

Figure S15. The IR spectrum of **V_{10}-CBTA**.

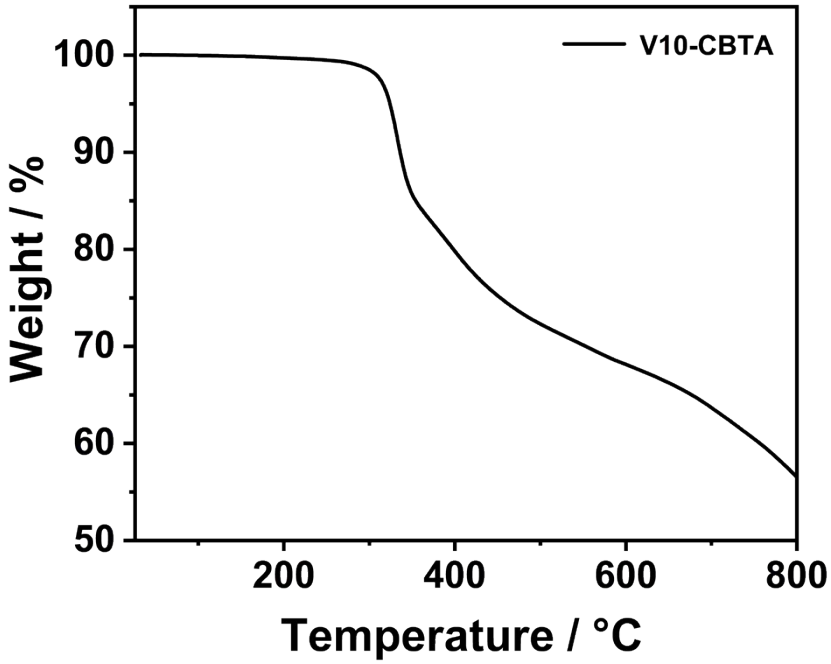

Figure S16. The TGA thermogram of as-synthesized **V_{10}-CBTA**.

4. Oxidation of Sulfides

To probe the catalytic reactivities of V_{10} clusters, we investigated the selective oxidation of sulfides. Thus, the oxidation of methyl phenyl sulfide (MPS) was selected as benchmark system to evaluate the activity of V_{10} clusters (Scheme S1). Preliminarily, a series of contrastive explorations for oxidation of the model MPS by using **V_{10}-BTA** as the catalyst were performed to obtain optimum reaction conditions (Figure S17). Obviously, the best catalytic effect could be attained when using 1% mol **V_{10}-BTA**, 1.5 eq hydrogen peroxide (H_2O_2) as the oxidant in 5 mL CH_3OH and at room temperature for 60 min. Under the aforementioned condition, **V_{10}-CBTA** also can catalyze the oxidation of MPS with commendable conversion, which shows better performance under even milder reaction conditions than some of the reported V-based heterogeneous catalysts.

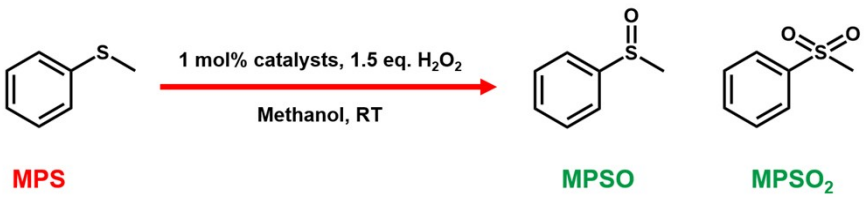

Scheme S1. Reaction Scheme for MPS Oxidation

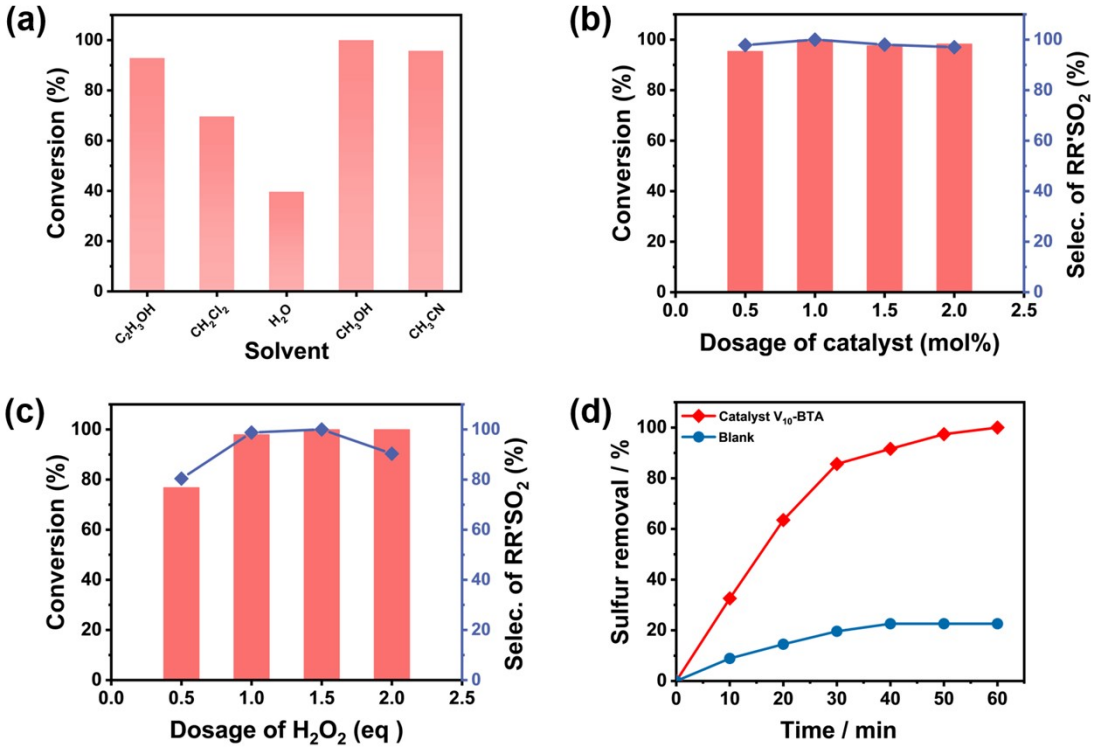

Figure S17. The relationships between the conversion/selectivity of oxidative products (RR'SO: methyl phenyl sulfoxide; RR'SO_2: methyl phenyl sulfone) and (a) the solvent, (b) the dosage of H_2O_2 (oxidant agent), (c) the dosage of catalyst **V_{10}-BTA**, and (d) the reaction time.

5. Benzene Hydroxylation to Phenol

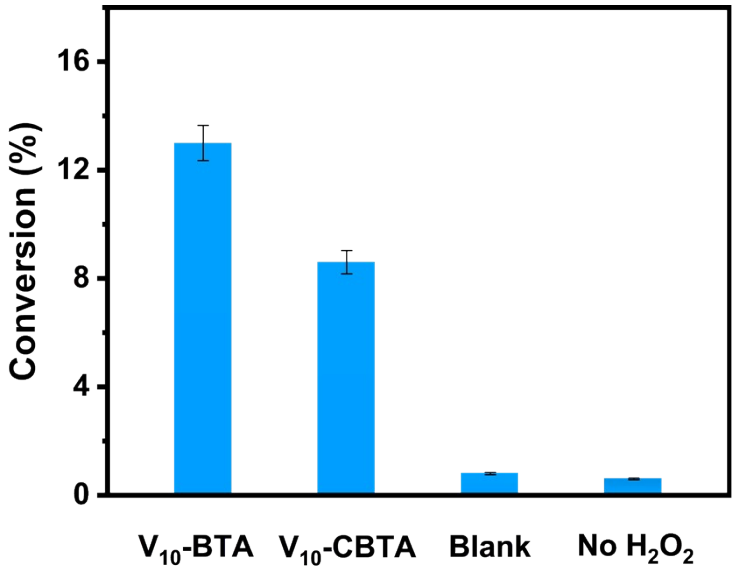

Figure S18. Catalytic oxidative reaction of benzene using **V_{10}-BTA** and **V_{10}-CBTA** as catalysts with respect to a catalyst-free (blank) and a H_2O_2-free trial. Reaction conditions: benzene (1 mL), 30% H_2O_2 (3 mL), catalyst (25 mg), CH_3CN (5.0 mL), 60 °C, 6 hours.

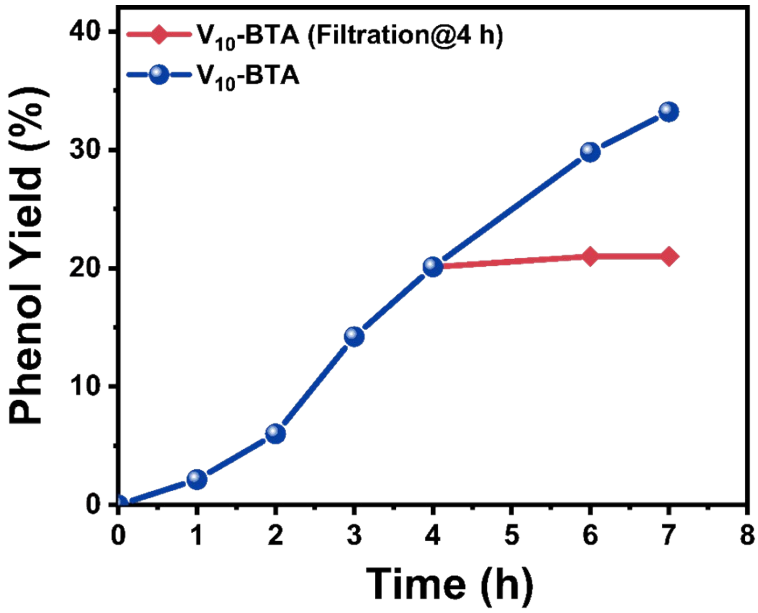

Figure S19. Catalytic dynamic of the hydroxylation of benzene by **V_{10}-BTA** (blue), and filter out the catalyst during the reaction (red).

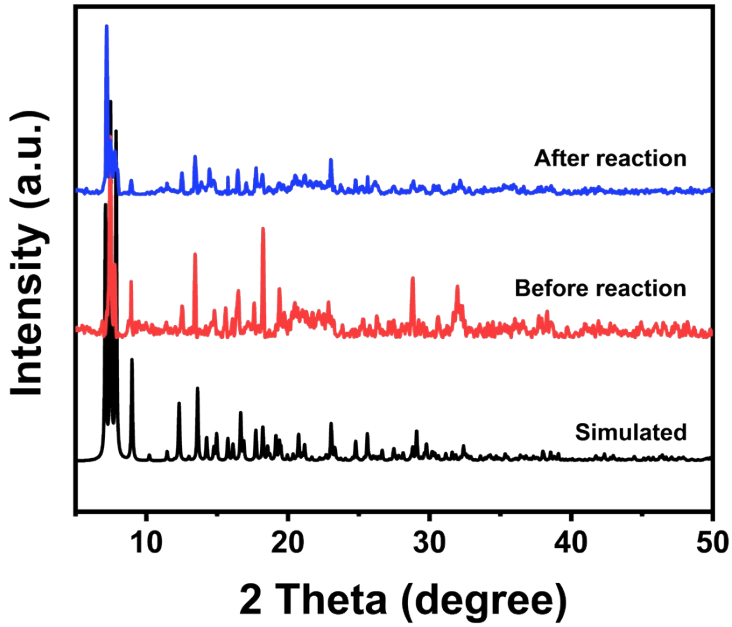

Figure S20. XRD pattern of **V_{10}-BTA** after several cycles in the hydroxylation of benzene.

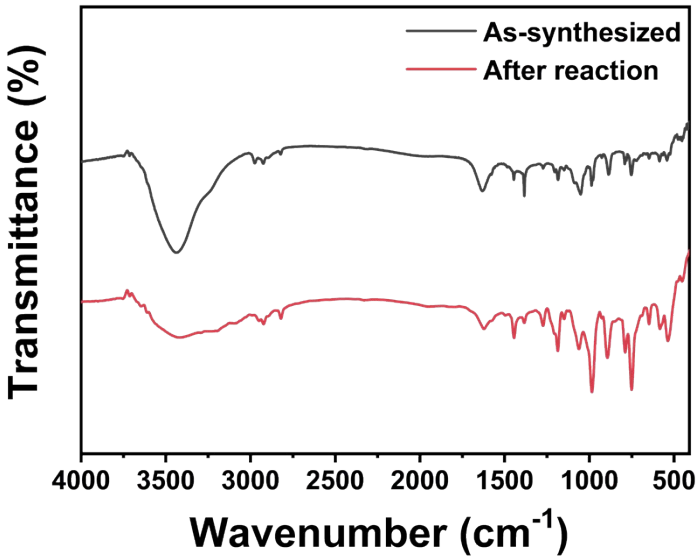

Figure S21. Infrared spectra of **V_{10}-BTA** after several cycles in the hydroxylation of benzene.

Table S5. The comparison of benzene hydroxylation of some reported POM-based catalysts.

Catalyst	Oxidant	Temperature (℃)	Phenol yield (%)	selectivity (%)	Ref.
V_{10}-BTA	**H_2O_2**	**60**	**32.2**	**99**	**This work**
$[Mo_2V_2O_9(bpy)_6][PMo_{11}VO_{40}]$	H_2O_2	80	25.5	90.7	[2]
$PMoV_2$/DMA16-CMPS	H_2O_2	65	21.9	99.3	[3]
$[Cu_{12}(BTC)_8(H_2O)_{12}][H_5PMo_{10}V_2O_{40}]$@ $49H_2O$	H_2O_2	65	13.4	93.4	[4]
$[DiBimCN]_2HPMoV_2$@NC-580	O_2	140	10.5	-	[5]
PMo_9V_3@ HKUST-1	O_2	80	7.4	99	[6]
POM@MOF-199@SBA-15	O_2	80	6	99	[7]
$\{[Fe^{II}(pyim)_2(C_2H_5O)][Fe^{II}(pyim)_2(H_2O)][PMo^{V}_2Mo^{VI}_9V^{IV}_3O_{42}]\}\cdot H_2O$	H_2O_2	60	16.2	94	[8]
C_3N_4-Ch_5PMoV_2	O_2	120	10.7	-	[9]

6. References

[1] I. D. Brown, D. Altermatt, Bond-Valence Parameters Obtained from a Systematic Analysis of the Inorganic Crystal Structure Database, *Acta Cryst. Section B*, **1985**, B41, 244-247.

[2] Hua Yang, Qing Wu, Jun Li, Wen Dai, Hengyun Zhang, Dan Lu, Shuang Gao, Wansheng You, Direct synthesis of phenol from benzene catalyzed by multi-V-POMs complex, *Applied Catalysis A: General*, **2013**, 457, 21-25.

[3] Hefang Wang, Luping Fang, Yongfang Yang, Li Zhang and Yanji Wang, $H_5PMo_{10}V_2O_{40}$ immobilized on functionalized chloromethylated polystyrene by electrostatic interactions: a highly efficient and recyclable heterogeneous catalyst for hydroxylation of benzene, *Catal. Sci. Technol.*, **2016**, 6, 8005-8015.

[4] Zeyu Du, Yanzhao Yu, Yalin Hong, Ningfang Li, Yemin Han, Jiapeng Cao, Qi Sun, Hua Mei, and Yan Xu, Polyoxometalate-Based Metal−Organic Frameworks with Unique High-Nuclearity Water Clusters, *ACS Appl. Mater. Interfaces*, **2020**, 12, 57174-57181.

[5] X. C. Cai, Q. Wang, Y. Q. Liu, J. Y. Xie, Z. Y. Long, Y. Zhou, J. Wang, Hybrid of Polyoxometalate-Based Ionic Salt and N-Doped Carbon toward Reductant-Free Aerobic Hydroxylation of Benzene to Phenol, *ACS Sustain. Chem. Eng.* **2016**, 4, 4986-4996.

[6] H. Yang, J. Li, L. Y. Wang, W. Dai, Y. Lv, S. Gao, Exceptional Activity for Direct Synthesis of Phenol from Benzene over PMoV@MOF with O_2, *Catal. Commun.* **2013**, 35, 101-104.

[7] H. Yang, J. Li, H.-Y. Zhang, Y. Lv, S. Gao, Facile Synthesis of POM@MOF Embedded in SBA-15 as a Steady Catalyst for the Hydroxylation of Benzene, *Microporous Mesoporous Mater.* 2014, 195, 87-91.

[8] Siman Li, Jilei Wang, Jiulin Zhou, Xinying Xiang, Yating Yu, Qun Chen, Hua Mei and Yan Xu, An iron-containing POM-based hybrid compound as a heterogeneous catalyst for one-step hydroxylation of benzene to phenol, *Dalton Trans.*, **2024**, 53, 1058-1065.

[9] Zhouyang Long, Guojian Chen, Sa Liu, Fangmin Huang, Liming Sun, Zhenglong Qin, Qian Wang, Yu Zhou, Jun Wang, Synergistic combination of graphitic C_3N_4 and polyoxometalate-based phase-transfer catalyst for highly efficient reductant-free aerobic hydroxylation of benzene, *Chem. Eng. J.*, **2018**, 334, 873-881.